Ultrashort-lived non-Rydberg doubly excited resonances in diatomic molecules

P. Erman, A. Karawajczyk, E. Rachlew-Källne, M. Stankiewicz,* and K. Yoshiki Franzén
Physics Department I, Royal Institute of Technology, S-10044 Stockholm, Sweden

P. Sannes and L. Veseth
Department of Physics, University of Oslo, N-0316 Oslo, Norway
(Received 3 December 1996)

The CO^+ emission systems A-X and B-X have been studied using monochromatic photon excitation in the range 20–34 eV. The vibrational branching ratios $(v'=4,5)/(v'=3,2)$ for the A-X system were found to remain essentially constant within this excitation range, while the $(v'=1,2)/(v'=0)$ branching ratios for the B-X system show a 40% variation. These results are interpreted using quasidegenerate many-body perturbation theory in terms of non-Rydberg doubly excited resonances in CO, which rapidly autoionize to various low-lying CO^+ states. It is suggested that some earlier observed variations in the photoionization branching ratios for the $v'=0$–2 levels of the CO^+ $X\,^2\Sigma^+$ have the same origin. [S1050-2947(97)02106-9]

PACS number(s): 33.80.Eh, 33.70.Jg

I. INTRODUCTION

In spite of the remarkable effort paid to studies of molecular valence-shell-excited configurations, very little is known about the properties of non-Rydberg doubly excited resonances (NRDER's). Although the existence of such states has been commonly anticipated, the first observation of NRDER's has been reported very recently [1], in contrast to the Rydberg-like doubly excited states, which have been extensively studied for almost twenty years (cf. Ref. [2] and references given therein). The small cross sections for photoabsorption to NRDER's, reflecting low probabilities for simultaneous excitation of two electrons, make the direct observation of such states most difficult in competition with photoabsorption to ''normal'' states. An additional obstacle to the detection of NRDER's is their very short lifetimes (of the order of 1 fs) giving rise to a natural broadening that is much larger than the vibrational separation. Thus, NRDER's may appear in the spectra in the form of broad irregular features that are difficult for unequivocal identification. Noticeably, subfemtosecond decay processes have not been observed in molecular physics and their occurrence actually reflects the high correlation of the electrons excited to the close-lying unoccupied valence states.

The electronic configurations of NRDER's, in which up to four shells may be simultaneously open, make their theoretical analysis a difficult task. The large number of interacting configurations in systems such as CO necessitates the use of rather elaborate models to compute the energies and a quasidegenerate many-body theory to second order was found to be both a practical and an efficient tool. In our recent work [1] such a formalism has already been shown to work in the case of the N_2 molecule. More specifically, five broad peaks were observed in the branching ratios $(v'=1)/(v'=0)$ of the N_2 (B-X) dispersed fluorescence (DF) following photoionization of N_2 in the 19–34 eV excitation range. From many-body perturbation calulations, four of these peaks could be identified with different attractive NRDER configurations formed by excitation of two inner-shell electrons to the closest, unoccupied valence states. These NRDER states rapidly autoionize into various vibrational levels of the N_2^+ $B\,^2\Sigma_u^-$ state, which changes the N_2^+ (B-X) emission. Variations in the N_2^+ (B-X) emission branching ratios at various photon excitation energies have also been observed earlier [3,4] but they were attributed to the interchannel coupling between the $3\sigma_g \rightarrow \epsilon\sigma_u$ shape resonance and $2\sigma_u \rightarrow \epsilon\sigma_g$ continuum. Our calculations also showed a number of repulsive NRDER states in N_2 that might decay by predissociation into neutral fragments rather than by autoionization. Actually, it was suggested [1] that two broad features observed in the fluorescence from neutral N fragments in photoionization of N_2 [5] originate from predissociation of two repulsive NRDER configurations. In the present work we have performed similar measurements on the isolectronic CO molecule. Previous studies of the $X\,^2\Sigma^+$ [6] and $B\,^2\Sigma^+$ [7] states of CO^+ have revealed a strong non-Franck-Condon behavior of vibrational branching ratios in the energy region 20–50 eV. The observed variations were ascribed to the interchannel coupling of the $4\sigma_u$ electron with the $5\sigma^{-1}$ shape resonances at an energy of about 29 eV and to the $4\sigma^{-1}$ shape resonance in the energy region 32–37 eV. However, such strong interchannel coupling should, in a similar way, affect the $5\sigma^{-1}$ channel for which no evidences have been found so far. In this work we intend to show that most of the observed effects may be explained in terms of autoionization from NRDER's in CO to the relevant CO^+ states.

II. STATEMENT OF THE PROBLEM

The basic objective of the present work is to measure vibrational branching ratios in the fluorescence from an excited molecular ionic state, following ionization of the neutral molecule by synchrotron radiation. If direct ionization is the only source of the fluorescence, then the branching ratios will be equal to the ratio σ_2/σ_1 of the vibrationally resolved

---

*Permanent address: Instytut Fizyki Mariana Smoluchowskiego, Jagiellonian University, Reymonta 4, Kraków, Poland.
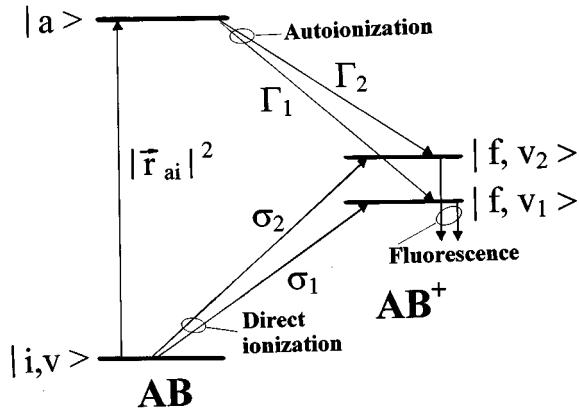
FIG. 1. Schematic description of the population of two vibrational levels $|f,v_1\rangle$ and $|f,v_2\rangle$ of an electronic state f in a molecular ion AB^+ created by direct photoionization from the ground state $|i,v\rangle$ as well as via autoionization from an upper state $|a\rangle$ in the neutral molecule AB. If only the direct process is present, the branching ratio σ_2/σ_1 of the fluorescence from f should be independent of the energy $h\nu$ of ionizing photons. However, when $h\nu$ is large enough to excite state $|a\rangle$, which autoionizes to the two vibrational levels $|f,v_1\rangle$ and $|f,v_2\rangle$ with partial rates Γ_1 and Γ_2, respectively, the fluorescence branching ratio is changed according to Eq. (1). This technique has been used for discovering NRDER states in N_2 [1] as well as in CO (present work).

cross sections (cf. Fig 1). However, there may be other processes that contribute to the observed branching ratios, in particular autoionization. Figure 1 gives a diagram of the combined process where the vibrational levels v_1 and v_2 of the fluorescent state $|f\rangle$ are assumed to be populated by direct ionization from the ground state $|i,v\rangle$ of the neutral molecule (cross sections σ_1 and σ_2, respectively) as well as being end products of the autoionization from an excited autoionizing state $|a\rangle$ (autoionization rates Γ_1 and Γ_2, respectively).

A rather straightforward derivation based on stationary conditions leads to the following expression for the branching ratio (B) for the the combined process:

$$B = \frac{\sigma_2}{\sigma_1}\left[1 + 4\pi^2\alpha\omega\,\frac{\Gamma_f}{\Gamma}\,\frac{|\vec{r}_{ai}|^2}{\sigma_f}\left(\frac{|\langle a|v_2\rangle|^2}{|\langle v|v_2\rangle|^2} - \frac{|\langle a|v_1\rangle|^2}{|\langle v|v_1\rangle|^2}\right)\right].$$
(1)

In the expression above, α is the fine-structure constant and ω the photon energy. Γ_f denotes the partial electronic autoionization rate from $|a\rangle$ to $|f\rangle$, and $\Gamma_1 = \Gamma_f|\langle a|v_1\rangle|^2$, $\Gamma_2 = \Gamma_f|\langle a|v_2\rangle|^2$. Γ represents the total rate of autoionization from $|a\rangle$ to all energetically allowed final states of the ion. In a similar way, σ_f represents the electronic cross section for ionization from the initial state $|i\rangle$ to the fluorescent state $|f\rangle$, and $\sigma_1 = \sigma_f|\langle v|v_1\rangle|^2$, $\sigma_2 = \sigma_f|\langle v|v_2\rangle|^2$. $|\vec{r}_{ai}|^2$ represents the electronic transition moment from $|i\rangle$ to $|a\rangle$, given by

$$|\vec{r}_{ai}|^2 = \tfrac{1}{3}(|\langle a|x|i\rangle|^2 + |\langle a|y|i\rangle|^2 + |\langle a|z|i\rangle|^2).$$

In Eq. (1) the relevant quantities have to be inserted in atomic units. The two terms in parentheses in Eq. (1) contain ratios of vibrational overlap integrals (Franck-Condon factors).

A basic assumption underlying the derivation of Eq. (1) is that the excited state $|a\rangle$ is decaying through autoionization only. The autoionization rate actually determines whether or not this condition is met. Later on (Sec. IV) we will present *ab intio* computations of Γ, and we will find that the associated lifetimes $\tau = 1/\Gamma$ are in the range 10^{-14}–10^{-15} s, which is too short for either predissociation or radiation to make a significant contribution.

Another assumption made by the derivation of Eq. (1) is that the effect of the autoionization is dominated by that of the direct ionization, so that the second term of Eq. (1) stays small compared to unity. From Eq. (1) we also see that the deviation from unity of the term in square brackets may, in priciple, be positive as well as negative, depending on the ratios of the relevant vibrational overlap integrals. An enhanced branching ratio is seen to occur when the population of the upper vibrational level v_2 via autoionization is relatively more efficient than for the lower level v_1. In Sec. III we will outline a method for *ab initio* computation of the partial rate of autoionization Γ_f, the total rate Γ, the transition moment $|\vec{r}_{ai}|^2$, as well as the excitation energies of the autoionizing states (resonances).

III. QUASIDEGENERATE MANY-BODY THEORY

In the present section, we shall give a brief outline of quasidegenerate many-body theory, which has been found to be an efficient tool for making *ab initio* predictions of central quantities of Eq. (1), i.e., Γ_f, Γ, $|\vec{r}_{ai}|^2$, and the excitation energy of the autoionizing states (resonances).

In the stationary Schrödinger equation of a many-body system,

$$H\Psi = E\Psi,$$
(2)

we partition the Hamiltonian H into an unperturbed part H_0 and a perturbation V,

$$H = H_0 + V.$$
(3)

Here H_0 is composed of one-body parts

$$H_0 = \sum_i [h(i) + u(i)]$$
(4)

and the perturbation V is defined by

$$V = \frac{1}{2}\sum_{i\neq j}\frac{1}{r_{ij}} - \sum_i u(i).$$
(5)

Solutions to the unperturbed problem (zeroth order)

$$H_0\Phi_i = E_i^{(0)}\Phi_i$$
(6)

form a complete set of Slater determinants $\{\Phi_i\}$, with corresponding energies $E_i^{(0)}$. In the present case we will face a situation with a rather large set of quasidegenerate zeroth-order states Φ_i, representing autoionizing states of proper symmetry in the experimentally interesting region. This set of states defines our model space P, and the remaining zeroth-order states compose the complementary or orthogo-

nal space Q. This division of our space of zeroth-order solutions is best described through the projection operators

$$P = \sum_{i \in P} |\Phi_i\rangle\langle\Phi_i|, \quad Q = 1 - P. \quad (7)$$

We now redefine our unperturbed Hamiltonian:

$$H_0^S = H_0 + \sum_{i \in P} (E_0 - H_0)|\Phi_i\rangle\langle\Phi_i| = H_0 + V_1, \quad (8)$$

which leads to

$$H_0^S \Phi_i = E_0 \Phi_i, \quad \text{all } i \in P,$$

where E_0 is an arbitrary reference energy. Thus, we see that the states in the model space P are exactly degenerate with respect to H_0^S.

In the next step, the Schrödinger equation (2) is transformed into an effective equation

$$H_{\text{eff}} P \Psi = E P \Psi, \quad (9)$$

where H_{eff} is given by a perturbation expansion:

$$H_{\text{eff}} = P H_0^S P + P(V - V_1)P$$
$$+ \sum_{i \in P} PV \frac{1}{E_i^{(0)} - H_0} QV|\Phi_i\rangle\langle\Phi_i| + \cdots . \quad (10)$$

The correct energies E of the system [cf. Eq. (2)] are now, in principle, obtained by diagonalizing the effective Hamiltonian matrix with elements

$$W_{kl} = \langle\Phi_k|H_{\text{eff}}|\Phi_l\rangle, \quad k, l \in P. \quad (11)$$

Through first order the elements of W are

$$W_{kl}^{(0)} + W_{kl}^{(1)} = E_0 \delta_{kl} + \langle\Phi_k|V - V_1|\Phi_l\rangle,$$

whereas the second-order contribution is [cf. Eq. (10)]

$$W_{kl}^{(2)} = \sum_{\beta \in Q} \langle\Phi_k|V|\beta\rangle\langle\beta|V|\Phi_l\rangle \frac{1}{E_l^{(0)} - E_\beta^{(0)}}. \quad (12)$$

The elements of $W^{(2)}$ are generally expressed in terms of diagrams, a topic that we shall not pursue further here. In the present investigation the perturbation expansion will be carried out through second order only. To second order there will be a total of 21 diagrams to include, whereas to the next (third) order there will be more than 200 diagrams. We believe that a second-order expansion will yield results of sufficient accuracy for the present analysis of experimental data. Carried through second order the quasidegenerate many-body theory yields an elegant as well as an efficient tool for making *ab initio* predictions of quantities relevant to the present study. The reader is referred to the literature [8–13] for further information on quasidegenerate many-body theory.

In the present work our model space will consist of a series of doubly excited configurations for the CO molecule. The corresponding states will be highly excited, and mainly decay via autoionization. A characteristic feature of an un-

stable, autoionizing state is that there is an imaginary contribution $-\frac{1}{2}i\Gamma$ to the energy, where Γ is the rate of autoionization. Furthermore, the lifetime τ of the state is given by $\tau = 1/\Gamma$. The imaginary part is actually inherent in the elements of the second-order matrix $W^{(2)}$ of Eq. (12). The process of autoionization is described by the occurrence of singular terms in the perturbation expansion. For such singular terms the states $|\beta\rangle$ of Eq. (12) will represent continuum states with a free outgoing electron. In that case the summation over β should be replaced by a complex integration and, according to standard rules for evaluating complex integrals, the singularity leads to an imaginary contribution [14–16].

In the present investigation the many-body method of [16] was implemented in the quasidegenerate procedure. The details of this implementation will, however, be given in a forthcoming paper. In this way, it was possible to obtain partial autoionization rates Γ_f for the doubly excited states of the model space [cf. Eq. (1)].

The next quantity to compute is the transition moment $|\vec{r}_{ai}|^2$ of Eq. (1). In the present case the transition is from the ground state in CO and up to doubly excited states. Thus the transition process will be a weak one, fully governed by correlation effects. Transition moments $|\vec{r}_{ai}|$ are included in the present approach by adding an operator equal to one of the molecule-fixed components (D_μ) of the electric dipole moment of the molecule to the perturbation V of Eq. (3). Thus, the perturbation V in the many-body expansion is replaced by $V + D_\mu$, and in Eq. (12) we will have cross terms that are first order in V as well as in D_μ. These cross terms will, in an indirect way, lead to the required transition moments with lowest-order correlation effects included. The details of this procedure will be postponed to a forthcoming paper.

At this point it should be noted that the matrix W of Eq. (11) will be non-Hermitian [cf. Eq. (12)]. This means that the eigenvectors of W or H_{eff} will be nonorthogonal. The eigenvectors are central to the process of computing transition moments, and for this purpose they need to be orthogonal [8]. To obtain this we will make an approximation that tends to be common in quasidegenerate perturbation theory (e.g., in nuclear physics [8]), i.e., W is replaced by the Hermitian matrix

$$\tfrac{1}{2}(W + \widetilde{W}).$$

In the present case this approximation turned out to have a rather insignificant effect on the eigenvalues to second order.

IV. NUMERICAL RESULTS

Only excited states of $^1\Sigma^+$ and $^1\Pi$ symmetry are accessible by electric-dipole transitions from the $X\,^1\Sigma^+$ ground state. The ground-state configuration of CO is $1\sigma^2 2\sigma^2 3\sigma^2 4\sigma^2 1\pi^4 5\sigma^2$, and our model space will consist of all configurations generated through all double excitations from the shells $4\sigma^2 1\pi^4 5\sigma^2$ to the excited orbitals 6σ, 7σ, and 2π. In addition, we also include single excitations from 3σ to 6σ, 7σ, and 2π, since the corresponding excited states are in the same energy range as the doubly excited ones. This leads to two separate noninteracting model spaces, one with a total of 29 states of $^1\Sigma^+$ symmetry, and another one actu-

TABLE I. Computed quantities relevant for autoionization to the $A\,^2\Pi$ excited state in CO^+ (see also Table III). Superscripts in the second column refer to curves in Fig. 2.

State	Excitation energy (eV)	$\lvert\vec{r}_{ai}\rvert^2$ (a.u.)	$\Gamma_f(A\,^2\Pi)$ (a.u.)	Γ (a.u.)	$\frac{\Gamma_f}{\Gamma}\lvert\vec{r}_{ai}\rvert^2$ (a.u.)	Lifetime $\tau=1/\Gamma$ (s)	Dominant configuration
$^1\Pi$	20.2	0.078	0.0076	0.0425	0.014	5.7×10^{-16}	$4\sigma^25\sigma1\pi^32\pi^2,$ $4\sigma5\sigma^21\pi^32\pi^2$(mix)
	20.8	0.012	0.0032	0.00791	0.0048	3.1×10^{-15}	"
	22.3	0.016	0.00032	0.00225	0.023	1.1×10^{-14}	$4\sigma^25\sigma^21\pi^22\pi6\sigma$
	23.2	0.021	0.0065	0.00679	0.020	3.6×10^{-15}	$4\sigma5\sigma^21\pi^32\pi^2$
	23.6	0.040	0.0018	0.00235	0.031	1.0×10^{-14}	$4\sigma^25\sigma^21\pi^22\pi\{^{6\sigma}_{7\sigma}$
	24.2[e]	0.11	0.0070	0.0071	0.11	3.4×10^{-15}	$4\sigma^25\sigma^21\pi^22\pi6\sigma$
	25.4[f]	0.32	0.0017	0.0018	0.30	1.3×10^{-14}	$4\sigma^25\sigma^21\pi^22\pi7\sigma$
	27.6[g]	0.036	0.0025	0.0032	0.028	7.6×10^{-15}	$4\sigma^25\sigma1\pi^36\sigma^2$
	29.7[h]	0.098	0.00013	0.00185	0.0067	1.3×10^{-14}	$4\sigma^{-2}5\sigma^21\pi^42\pi7\sigma$
$^1\Sigma^+$	34.9	0.0095	0.0026	0.00509	0.0049	4.8×10^{-15}	$3\sigma4\sigma^25\sigma^21\pi^46\sigma$
	35.9[5]	0.146	0.00049	0.00181	0.040	1.3×10^{-14}	$3\sigma4\sigma^25\sigma^21\pi^47\sigma$

ally with the same number of $^1\Pi$ states.

The orbitals used for the model space were obtained from a Hartree-Fock calculation for the $^1\Pi$ state derived from the doubly excited configuration $1\sigma^22\sigma^23\sigma^24\sigma^21\pi^35\sigma6\sigma^2$. Thus we start out with most of the orbitals optimized for the energy range in question. The ground-state energy was also calculated with this set of orbitals and, to second order, there was no significant deviation from the energy obtained with orbitals optimized for the ground state. The excited orbitals included in the model space were restricted to the 6σ, 7σ, and 2π orbitals for several reasons. The 6σ and 2π orbitals have negative orbital energies, i.e., bound states, and the orbital energy of the 7σ is also low (0.005 a.u.). Furthermore, all three of these orbitals are clearly localized, i.e., of valence type, whereas the higher σ and π orbitals with low orbital energies are much more delocalized, i.e., Rydberg-type orbitals. Finally, the model space tends to grow to intractable sizes if more excited orbitals are included.

The basis sets of atomic orbitals used for the present calculations were extensions of the set of Slater orbitals with optimized exponents published by Cade and Huo [17]. Several diffuse $2s$, $2p$, and $3d$ orbitals were added to make some allowance for Rydberg orbitals. Finally, a set of 11 ∂ orbitals based on $3d$ orbitals in O and C were included in the configurations representing the orthogonal Q space. All calculations were carried out at the equilibrium internuclear separation $R_e=2.132$ a.u. for the CO ground state, i.e., only vertical transitions are considered.

Some representative results of the calculations are shown in Tables I–III. Here we list the computed excitation energies (with reference to the second-order ground-state energy), the transition probabilities $\lvert\vec{r}_{ai}\rvert^2$, the total autoionization rate Γ, and the partial autoionization rate Γ_f to the $A\,^2\Pi$, $B\,^2\Sigma^+$, and $X\,^2\Sigma^+$ states in CO^+. We also list the quantity $\lvert\vec{r}_{ai}\rvert^2(\Gamma_f/\Gamma)$, which is of basic importance for the variation of the branching ratios. In the tables we have in-

TABLE II. Computed quantities relevant for autoionization to the $B\,^2\Sigma^+$ excited state in CO^+ (see also Table III).

State	Excitation energy (eV)	$\lvert\vec{r}_{ai}\rvert^2$ (a.u.)	$\Gamma_f(B\,^2\Sigma^+)$ (a.u.)	Γ (a.u.)	$\frac{\Gamma_f}{\Gamma}\lvert\vec{r}_{ai}\rvert^2$ (a.u.)	Lifetime $\tau=1/\Gamma$ (s)	Dominant configuration
$^1\Pi$	22.3[b]	0.016	0.0012	0.00225	0.0086	1.1×10^{-14}	$4\sigma^25\sigma^21\pi^22\pi6\sigma$
	23.3[c]	0.040	0.00064	0.00165	0.016	1.5×10^{-14}	$4\sigma5\sigma1\pi^42\pi7\sigma$
	23.6[d]	0.040	0.00029	0.00235	0.0050	1.0×10^{-14}	$4\sigma^25\sigma^21\pi^22\pi\{^{6\sigma}_{7\sigma}$
	24.9	0.0070	0.00072	0.00123	0.0041	2.0×10^{-14}	strong configuration interaction
	25.4[f]	0.32	0.000052	0.00178	0.0094	1.4×10^{-14}	$4\sigma^25\sigma^21\pi^22\pi7\sigma$
	28.4	0.0066	0.0015	0.00257	0.0040	9.4×10^{-15}	$4\sigma^{-2}5\sigma^21\pi^42\pi6\sigma$
	29.7[h]	0.098	0.00041	0.00185	0.022	1.3×10^{-14}	$4\sigma^{-2}5\sigma^21\pi^42\pi7\sigma$
$^1\Sigma^+$	23.6[1]	0.018	0.0011	0.00290	0.0068	8.3×10^{-15}	$4\sigma5\sigma^21\pi^32\pi7\sigma$
	24.4[2]	0.010	0.0056	0.00912	0.0063	2.6×10^{-15}	strong configuration interaction
	27.3[4]	0.026	0.00021	0.00126	0.0044	1.9×10^{-14}	$4\sigma^25\sigma^{-2}1\pi^46\sigma7\sigma$
	35.9[5]	0.146	0.00060	0.00181	0.048	1.3×10^{-14}	$3\sigma4\sigma^25\sigma^21\pi^47\sigma$

TABLE III. Computed values relating to excited states of $^1\Pi$ and $^1\Sigma^+$ symmetries, respectively, in CO, and to autoionization to the CO^+ X $^2\Sigma^+$ ground state.

State	Excitation energy (eV)	$|\vec{r}_{ai}|^2$ (a.u.)	$\Gamma_f(X\,^2\Sigma^+)$ (a.u.)	Γ (a.u.)	$\frac{\Gamma_f}{\Gamma}|\vec{r}_{ai}|^2$ (a.u.)	Lifetime $\tau=1/\Gamma$ (s)	Dominant configuration
$^1\Pi$	16.5	0.016	0.019	0.0346	0.0085	7.0×10^{-16}	$4\sigma^2 5\sigma 1\pi^3 2\pi^2$
	18.1	0.0071	0.011	0.0177	0.012	1.4×10^{-15}	$4\sigma^2 5\sigma^{-2} 1\pi^4 2\pi 6\sigma$
	18.6	0.013	0.0014	0.00157	0.012	1.5×10^{-14}	$4\sigma^2 5\sigma^{-2} 1\pi^4 2\pi 7\sigma$
	20.2	0.078	0.018	0.0425	0.033	5.7×10^{-16}	$4\sigma^2 5\sigma 1\pi^3 2\pi^2,$ $4\sigma 5\sigma^2 1\pi^3 2\pi^2(\text{mix})$
	$20.8^{(a)}$	0.012	0.0045	0.00791	0.0068	3.1×10^{-15}	$''$
	$22.3^{(b)}$	0.016	0.00073	0.00225	0.0052	1.1×10^{-14}	$4\sigma^2 5\sigma^2 1\pi^2 2\pi 6\sigma$
	$23.3^{(c)}$	0.040	0.00088	0.00165	0.0214	1.5×10^{-14}	$4\sigma 5\sigma 1\pi^4 2\pi 7\sigma$
	$23.6^{(d)}$	0.040	0.00022	0.00235	0.0038	1.0×10^{-14}	$4\sigma^2 5\sigma^2 1\pi^2 2\pi\{^{6\sigma}_{7\sigma}$
$^1\Sigma^+$	$23.6^{(1)}$	0.018	0.0014	0.0029	0.0083	8.3×10^{-15}	$4\sigma 5\sigma^2 1\pi^3 2\pi 7\sigma$
	$26.6^{(3)}$	0.032	0.0069	0.0087	0.026	2.8×10^{-15}	$4\sigma^2 5\sigma^{-2} 1\pi^4 6\sigma^2$
	$27.3^{(4)}$	0.026	0.00086	0.00126	0.018	1.9×10^{-14}	$4\sigma^2 5\sigma^{-2} 1\pi^4 6\sigma 7\sigma$
	28.5	0.020	0.00018	0.00060	0.0060	4.0×10^{-14}	$4\sigma^2 5\sigma^{-2} 1\pi^4 7\sigma^2$
	$35.9^{(5)}$	0.146	0.000094	0.00181	0.0076	1.3×10^{-14}	$3\sigma 4\sigma^2 5\sigma^2 1\pi^4 7\sigma$

cluded only those excited states for which the value of this quantity is 0.0040 a.u. or larger. From Eq. (1) we can conclude that even with the most favorable vibrational overlappings, values smaller than 0.0040 a.u. will lead to variations in the branching ratios that are smaller than 1–2 %. For most of the excited states the value of $|\vec{r}_{ai}|^2(\Gamma_f/\Gamma)$ is much smaller than 0.004 a.u. and they will consequently not contribute to any observable deviation of the branching ratio from that of the direct ionization.

Finally, it should be mentioned that the excitation energies of the 29 $^1\Sigma^+$ states and the 29 $^1\Pi$ states considered are rather evenly distributed in the range 15.5–40.7 eV. Potential curves for internuclear separations in the range 1.85–2.60 a.u. are shown in Fig. 2 for a selection of the $^1\Pi$ and

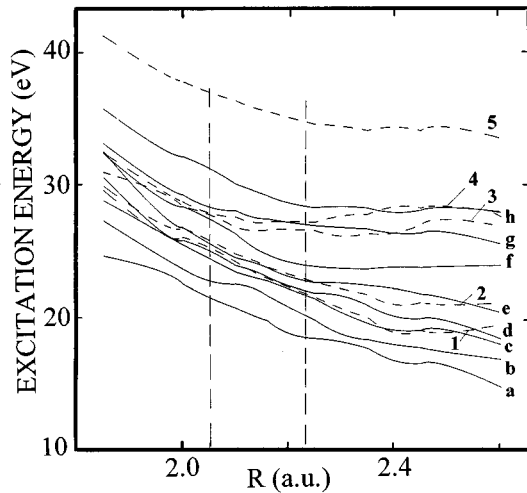FIG. 2. Calculated potential-energy curves of $^1\Sigma^+$ and $^1\Pi$ NRDER's in CO with significant contributions to measured branching ratios. Solid lines, $^1\Pi$ states; dashed lines, $^1\Sigma^+$ states. Letters and numbers on the potential curves refer to the entries in Tables I–III (cf. excitation energies).
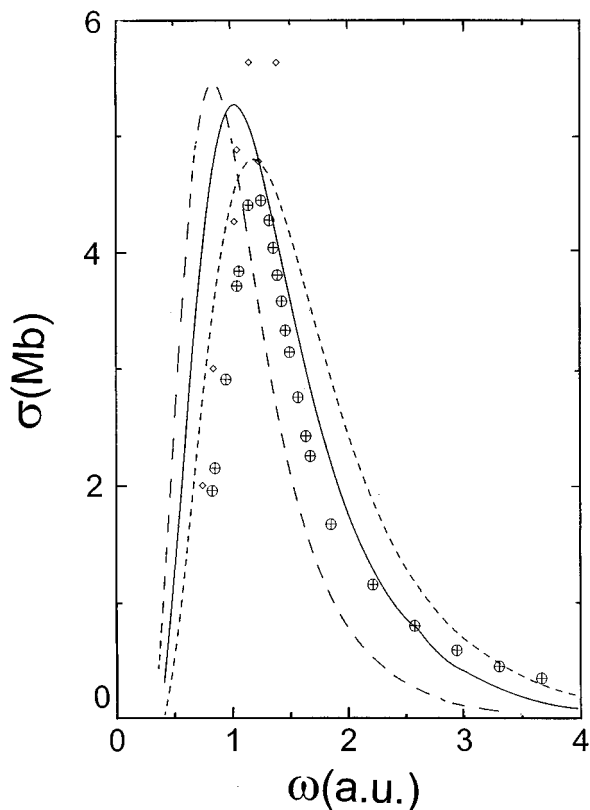
$^1\Sigma^+$ states that tend to make important contributions to the branching ratio.

We have also computed the partial cross section for direct ionization to the B $^2\Sigma^+$ state in CO^+, which is of particular interest for the present investigation. The cross sections were computed by use of many-body theory [18,19], and the results obtained at three different internuclear separations are shown in Fig. 3, where experimental results are also included for comparison [20,21]. Cross sections were actually computed for a series of internuclear separations in the range 1.85–2.40 a.u. These results were then combined with vibrational wave functions obtained from Rydberg-Klein-Rees (RKR) potential curves for the CO ground state and the CO^+ B $^2\Sigma^+$ state [22,23] to compute vibrationally resolved cross sections. Thus we obtain an *ab initio* value for the leading term σ_2/σ_1 in Eq. (1) for the branching ratio. The result of this calculation is shown in Fig. 5. There is seen to be a significant difference between our new *ab initio* ratio and the constant ratio obtained from the Franck-Condon approximation.

V. EXPERIMENT

The experimental equipment was the same as in our N_2 experiment [1]. In short, synchrotron light from the MAX storage ring in Lund, monochromatized to about 0.4 nm in the 20–34 eV range, excited CO gas at about 3×10^{-2} Torr and the CO^+ B $^2\Sigma$–X $^2\Sigma^+$ fluorescence was detected using an $f=19$ cm grating spectrometer equipped with a position-sensitive, liquid-nitrogen–cooled charge-coupled-device array detector. The resolution of the spectrometer was set to 1.5 nm and the spectral coverage was 170–470 nm. The studied spectral range covers the most prominent features of the two emission systems CO^+ $(A$ $^2\Pi$–X $^2\Sigma^+)$ and CO^+ $(B$ $^2\Sigma^+$–X $^2\Sigma^+)$. The vibrational structure is well resolved for the whole A-X system and for the B-X $\Delta v=2$ sequence. The A-X (5;0), (4;0), (3;0), and (2;0) bands and the B-X (0;2), (1;3), and (2;4)

FIG. 3. Partial cross sections for ionization to the CO^+ B $^2\Sigma^+$ state computed at three different internuclear separations using the many-body theory. Experimental results [20,21] are included for comparison. Long-dashed line, $R = 2.40$ a.u.; solid line, $R = 2.132$ a.u., short-dashed line, $R = 1.85$ a.u., experimental points $\otimes$ [20], and $\diamond$ [21].

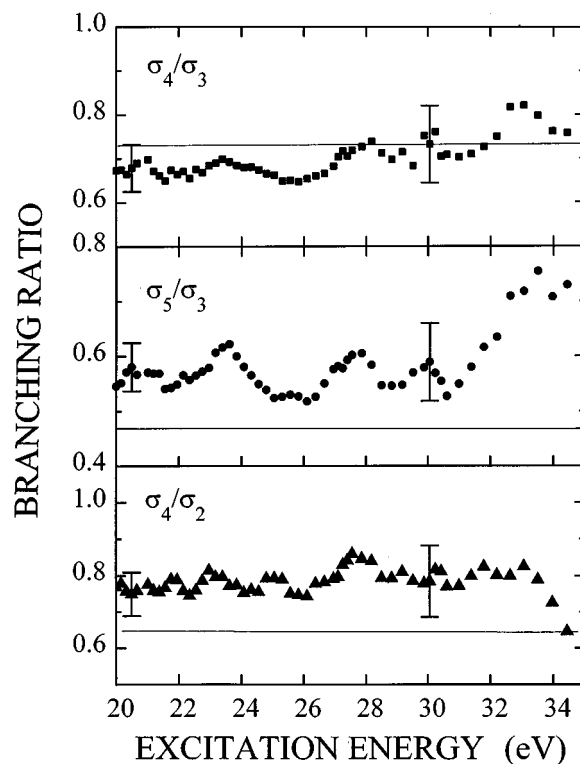

FIG. 4. Measured branching ratios of the relative population of various denoted vibrational levels of the CO^+ A $^2\Pi$ state as a function of the energy $h\nu$ of the exciting photons. The energy-dependent experimental errors are indicated at 20.5 and 30 eV and the experimental points are displayed using three-point smoothing. The ratios of the corresponding Franck-Condon factors for ionizing transitions from the CO ground state are indicated as solid lines in the three cases.

bands were selected for the relative intensity measurements from which the corresponding branching ratios were directly obtained by division with the associated Franck-Condon factors.

VI. RESULTS AND DISCUSSION

Figures 4 and 5 show the deduced vibrational branching ratios as a function of the excitation energy $h\nu$, for the CO^+ A $^2\Pi$ and CO^+ B $^2\Sigma^+$ states, respectively. As seen from Fig. 4, the branching ratios σ_4/σ_3, σ_5/σ_3, and σ_4/σ_2 of the CO^+ A $^2\Pi$ state remain essentially constant in the excitation range 20–32 eV. Moreover, all the measured ratios are in fair agreement with the respective ratios of the Franck-Condon factors for ionizing transitions from the CO ground state $q[\text{CO } X \rightarrow \text{CO}^+ \ A(v'=4,5)]/q[\text{CO } X \rightarrow \text{CO}^+ \ A(v'=2,3)]$ which are 0.73, 0.47, and 0.64 for σ_4/σ_3, σ_5/σ_3, and σ_4/σ_2, respectively. The variations of the branching ratios at about 23 eV and 28–30 eV excitation energy are within the experimental error (estimated for 8% at $h\nu=20$ eV and 12% at $h\nu=30$ eV) while the deviation of the branching ratio from the Franck-Condon level observed for $h\nu\geq31$ eV is probably significant.

In contrast to the weak changes seen in Fig. 4, the branching ratios σ_1/σ_0 and σ_2/σ_0 for the $(v'=1,2)/(v'=0)$ CO^+ $(B$ $^2\Sigma^+-X$ $^2\Sigma^+)$ emission (Fig.

5) both show a strong variation with $h\nu$ and a deviation from the calculated ratios of the Franck-Condon factors for ionization from the CO ground state (0.34 and 0.065, respectively). Clearly, the observed deviations from the Franck-Condon levels shown in Fig. 5 (top) are much larger than the experimental error, which increases with the excitation energy from 5% at $h\nu=20$ eV up to 8% at $h\nu=30$ eV (Fig. 5, top) and 10% at $h\nu=20$ eV up to 25% at $h\nu=30$ eV (Fig. 5, bottom). Additionally, in Fig. 5 (top) the dashed curve shows the result of our *ab inito* calculations of the ratio σ_1/σ_0 of the vibrationally resolved cross sections, as discussed in Sec. IV. Thus higher vibrational states are overpopulated with respect to the Franck-Condon value as well as to our new nonconstant *ab initio* results around a broad peak at $h\nu \sim 22$ eV and $h\nu\geq25$ eV (Fig. 5, top).

Before attributing the observed variations to autoionization of NRDER states in CO, we have to show that they do not originate from decays of upper, "ordinary" CO^+ states. Actually, high-resolution photoelectron spectroscopy [24] has recently revealed that there are two CO^+ states in the 22–24 eV range, namely D $^2\Pi$ at 22.38 eV ($v'=0$), 22.56 eV ($v'=1$), 22.73 eV ($v'=2$), ..., and 3 $^2\Sigma^+$ at 22.99 eV ($v'=0$), 23.20 eV ($v'=1$), 23.39 eV ($v'=2$), ... Another CO^+ state, C $^2\Delta$ at 21.70 eV ($v'=0$) is known from emission spectroscopy [25], but since photon excitation to this state from the CO $^1\Sigma^+$ ground state and C $^2\Delta$
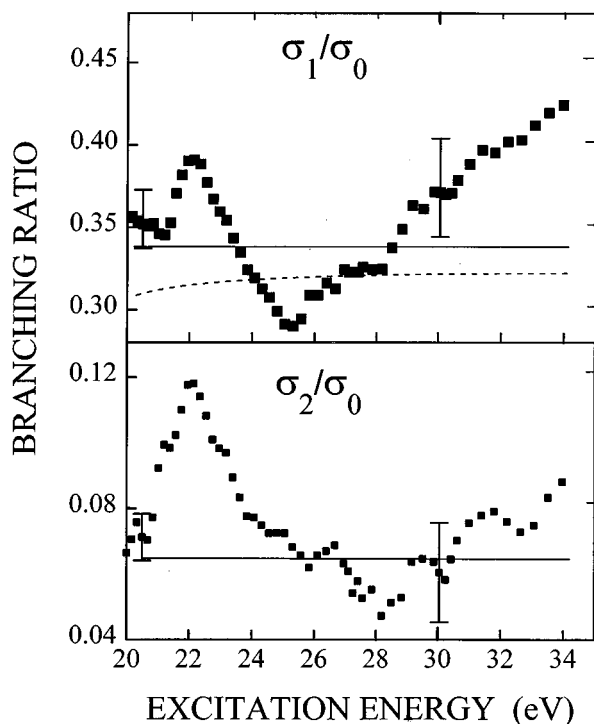
FIG. 5. Measured branching ratios of the relative populations of various denoted vibrational levels of the CO$^+$ B $^2\Sigma^+$ displayed in the same way as for the CO$^+$ A $^2\Pi$ state (Fig. 4). The dashed line in Fig. 5 (top) follows from *ab initio* calculations of σ_1/σ_0 as described in Sec. IV.

$-B$ $^2\Sigma^+$ emission are both forbidden processes, the C $^2\Delta$ state may be left out of consideration. However, we must seriously consider the intensity of the allowed emissions CO$^+$ (D $^2\Pi$–B $^2\Sigma^+$) and CO$^+$ (3 $^2\Sigma^+$–B $^2\Sigma^+$), which could possibly be the origin of the structure around 22–24 eV in Fig. 5. If this emission occurs, it should be very weak since it has never been observed in emission spectroscopy of CO$^+$ in spite of extensive studies during the past decades. A more quantitative estimate may be obtained from the high-resolution photoelectron spectrum [24], which shows that the intensity ratio between the strongest populated D-state level and the $B(v'=1)$ level is less than 2%. Moreover, since the energy ratio $[\Delta E(D\text{-}B)/\Delta E(D\text{-}X)]^3 \sim 1/30$, 97% of all excited D levels would decay to CO$^+$ $X^2\Sigma^+$ and only 3% to CO$^+$ B $^2\Sigma^+$. This indicates that less than 0.1% of the populations of the B-state levels could be created via cascades from the D state. Analogous arguments exclude cascades from the CO$^+$ 3 $^2\Sigma^+$ state as the origin of the structure around 22–24 eV in Fig. 5. Thus, we conclude that this peak and the remaining structure in Fig. 5 has another origin and, in view of our N$_2$ studies [1] and the present calculations, we suggest that the structure follows from autoionization of upper NRDER CO states.

The identification of the structure observed in the vibrational branching ratio (Figs. 4 and 5) is based on our calculations of the NRDER's performed as described in Secs. III and IV. The results presented in Table I reveal six states whose transition probabilities $(\Gamma_f/\Gamma)|\vec{r}_{ai}|^2$ would, in principle, allow for their observation in Fig. 4. However, the short lifetime of these NRDER's suggest that the autoioniz-

ation to the A $^2\Pi$ state occurs within the same Franck-Condon region as the excitation process ($R_e=2.13$ a.u.). In fact, this strongly disadvantages the decay to the A $^2\Pi$ level, whose potential curve is significantly shifted (0.23 a.u.) towards larger internuclear distances with respect to the ground state of CO. Moreover, most of the calculated NRDER's are nonbonding states and thus efficient excitation to these levels occurs at the low internuclear distances (close to the potential curve). Importantly, the transition probabilities from the NRDER's to the states with shifted potential curves may be additionally reduced by interference effects. Since most of the NRDER's are repulsive (see Fig. 2) and their natural width is large, the excitation occurs simultaneously to several vibrational (or continuum) sublevels of the NRDER's. Due to the short lifetime, the autoionization to the lower-lying states takes place before the coherence induced between the excited levels is lost. It may be shown that for transitions to higher vibrational levels of the final state (which are strong in view of the different equilibrium distances) the respective matrix elements may appear with opposite signs. Summing up the partial transition probabilities for deexcitation from the various sublevels of the NRDER's, strong destructive interference effects are observed that may reduce the final transition probabilities by orders of magnitude. More detailed studies of this effect are in progress. Nothing has been found that may explain in terms of NRDER's the apparent variations of the experimental curve above 31 eV. We will come back to this point later in the paper.

Table II contains the list of the NRDER's strongly decaying to the B $^2\Sigma^+$ state of CO$^+$. Clearly the pronounced peak at 22 eV coincides with the calculated position of the $^1\Pi$ state (leading configuration $1\pi^2 2\pi 6\sigma$). Additionally, two $^1\Pi$ and one $^1\Sigma^+$ states have been found at 23.3 eV, 23.6 eV, and 23.6 eV, respectively, which may explain the asymmetric shape of the feature observed in Fig. 5 in the energy range 22–24 eV.

The dip at 24–26 eV may be attributed to the three overlapping NRDER states (two $^1\Pi$ states found at 24.9 and 25.4 eV, and a single $^1\Sigma^+$ state at 24.4 eV). The energy separation that is comparable to their lifetime broadening prevents their distinct observation.

The observed continuous growth of the σ_1/σ_0 curve above $h\nu=31$ eV is puzzling. Although two $^1\Pi$ states at 28.4 eV and 29.7 eV and one $^1\Sigma^+$ state at 27.3 eV may explain the increase of the branching ratio above the Franck-Condon level at 28–30 eV, the calculated NRDER's do not provide the explanation for $h\nu>31$ eV. Slightly outside the energy range of the present investigation there is an important singly excited $(3\sigma\rightarrow7\sigma)$ $^1\Sigma^+$ state at 35.9 eV. We shall compare this effect with the weak but probably significant variations of the branching ratio of the A $^2\Pi$ state in the considered energy region.

The recent photoelectron data [24] reveal a group of transitions to various vibrational levels of a singly excited CO$^+$ state (e.g., 4 $^2\Sigma^+$ with the leading configuration $3\sigma^{-1}$) between 31 and 36 eV. Obviously, there should exist a number of neutral Rydberg series converging to CO$^+$ (4 $^2\Sigma^+$,v) which may autoionize into both the A $^2\Pi$ and the B $^2\Sigma^+$ state of CO$^+$ and influence the measured vibrational population. Since the NRDER's must be excluded in the energy
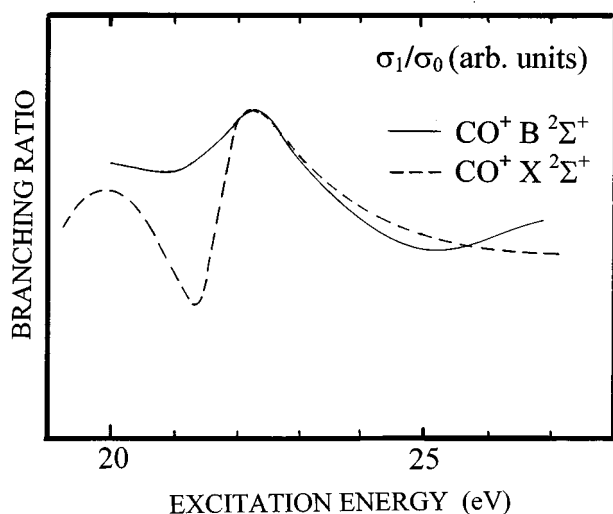
FIG. 6. Measured branching ratios σ_1/σ_0 for the CO^+ X $^2\Sigma^+$ state [6] and CO^+ B $^2\Sigma^+$ state (present work). The similarity between the two curves suggests that their shapes have the same origin, i.e., autoionizations from NRDER states in CO.

range 30–35 eV in view of the theoretical analysis (Tables I and II), the experimentally observed non-Franck-Condon behavior in this range is probably due to autoionization of these (doubly excited) Rydberg series.

A comparison of the shapes of the potential curves of the ground X $^2\Sigma^+$ and B $^2\Sigma^+$ states show that both of them lie in the same Franck-Condon region. Thus some of the NRDER's that strongly decay to the B $^2\Sigma^+$ state should also partially autoionize to the X $^2\Sigma^+$ state. Previous photoelectron studies [6] of the vibrational branching ratio of the ground electronic state of the CO^+ molecule revealed a structure at $h\nu = 19$–22 eV excitation energy that had been originally attributed to the 5σ shape resonance. However, the observed features could not be reproduced by Hartree-Fock calculations [26] or multiple scattering methods [27]. It was proposed that autoionizing states may account for the observed peaks in the branching ratios. In Fig. 6 the measured branching ratio σ_1/σ_0 of the CO^+ X $^2\Sigma^+$ state [6] is displayed as a dashed line together with the presently measured σ_1/σ_0 ratio for the CO^+ B $^2\Sigma^+$ state (Fig. 5, top). Notice-

ably, the shapes of the two curves are very similar.

Moreover, we have applied the formalism presented earlier in this paper in order to calculate NRDER's, which may decay to the ground-state continuum with sufficiently large probability. Our results (see Table III) show the existence of the $^1\Pi$ states at 20.2 eV and 23.2 eV, which strongly autoionize into the X $^2\Sigma^+$ level. The excellent agreement of the calculations with the photoelectron spectra as well as the striking similarity between both experimental curves (Fig. 6) strongly support the explanation in terms of autoionization from presently computed NRDER's. Additonally, we have calculated the energies and potential curves of all NRDER's that may efficiently autoionize to the X $^2\Sigma^+$ state in the energy range up to 35 eV (cf. Table III).

VII. CONCLUSIONS

To summarize, the present work reveals the existence of non-Rydberg doubly excited resonances in the energy region 20–35 eV in the CO molecule that, to our knowledge, have escaped previous observation. In the present work NRDER's have been indirectly observed by monitoring their decay to lower-lying states of the CO^+ ion. Features observed in the vibrational branching ratio of the B $^2\Sigma^+$ state of CO^+ have been compared to the results of theoretical calculations showing very good agreement. Since the discovered states may only weakly decay to the A $^2\Pi$ level, the vibrational branching ratios of this state should not deviate from the Franck-Condon behavior. We have experimentally confirmed this expectation. Finally, we have studied theoretically NRDER's that may strongly autoionize to the ground CO^+ X $^2\Sigma^+$ state. An excellent agreement between the energy of the computed states and the previously published experimental data suggest that the recorded structure originates from the decay of NRDER's rather than from the 5σ continuum coupling, as previously suggested.

[1] P. Erman, A. Karawajczyk, U. Köble, E. Rachlew-Källne, K. Yoshiki Franzen, and L. Veseth, Phys. Rev. Lett. **76**, 4136 (1996).

[2] M. Ukai, K. Kameta, N. Kouchi, and Y. Hatano, Phys. Rev. A **46**, 7019 (1992).

[3] A. Dadouch, G. Dujardin, L. Hellner, M. J. Besnard-Ramage, and B. J. Olsson, Phys. Rev. A **43**, 6057 (1991).

[4] E. D. Poliakoff, M.-H. Ho, G. E. Leroi, and M. G. White, J. Chem. Phys. **84**, 4779 (1986).

[5] E. D. Poliakoff, S. Kakar, and R. A. Rosenberg, J. Chem. Phys. **96**, 2740 (1992).

[6] R. Stockbauer, B. Cole, D. L. Ederer, J. B. West, A. C. Parr, and J. L. Dehmer, Phys. Rev. Lett. **43**, 757 (1979).

[7] S. Kakar, H. C. Choi, and E. D. Poliakoff, Chem. Phys. Lett. **190**, 489 (1992).

[8] B. H. Brandow, Adv. Quantum Chem. **10**, 187 (1977).

[9] G. Hose and U. Kaldor, J. Phys. B **12**, 3827 (1979).

[10] G. Hose and U. Kaldor, Phys. Scr. **21**, 357 (1980).

[11] G. Hose and U. Kaldor, J. Phys. Chem. **86**, 2133 (1982).

[12] U. Kaldor, J. Chem. Phys. **81**, 2406 (1984).

[13] S. Kucharski and R. J. Bartlett, Int. J. Quantum Chem. Quantum Chem. Symp. **22**, 383 (1988).

[14] H. P. Kelly, Phys. Rev. A **11**, 556 (1975).

[15] T. Von Åberg, G. Howat, L. Karlsson, J. A. R. Samson, H. Siegbahn, and H. Starace, *Corpuscles and Radiation in Matter I*, edited by W. Mehlhorn, Handbuch der Physik Vol. 31

(Springer-Verlag, Berlin, 1982), p. 469.

[16] L. Veseth, J. Phys. B **29**, 977 (1996).

[17] P. E. Cade and W. M. Huo, At. Data Nucl. Data Tables **15**, 1 (1975).

[18] L. Veseth, Phys. Rev. A **44**, 358 (1991).

[19] L. Veseth, Phys. Rev. A **49**, 939 (1994).

[20] O. Hemmers (private communication).

[21] E. W. Plummer, T. Gustafsson, W. Gudat, and D. E. Eastman, Phys. Rev. A **15**, 2339 (1977).

[22] I. Tobias, R. J. Fallon, and J. T. Vanderslice, J. Chem. Phys. **33**, 1638 (1960).

[23] R. B. Singh and D. K. Rai, J. Mol. Spectrosc. **19**, 424 (1966).

[24] P. Baltzer, M. Lundqvist, B. Wannberg, L. Karlsson, M. Larsson, M. A. Hayes, J. B. West, M. R. F. Siggle, A. C. Parr, and J. L. Dehmer, J. Phys. B **27**, 4915 (1994).

[25] J. Marchaud, J. d'Incan, and J. Janin, Spectrochim. Acta A **25**, 605 (1969).

[26] M. Smith, D. Lynch, and V. McKoy, J. Chem. Phys. **85**, 6455 (1982).

[27] J. A. Stephens, D. Dill, and J. L. Dehmer, J. Phys. B **14**, 3911 (1981).